

Oxygen-rich dust production in IC 10[★]

V. Leboutteiller^{1,2}, G. C. Sloan², M. A. T. Groenewegen³, M. Matsuura⁴, D. Riebel^{5,6}, D. G. Whelan⁷,
J. Bernard-Salas⁸, P. Massey⁹, and E. Bayet¹⁰

¹ Laboratoire AIM, CEA/DSM-CNRS-Université Paris Diderot DAPNIA/Service d'Astrophysique, Bât. 709, CEA-Saclay, 91191 Gif-sur-Yvette Cedex, France

e-mail: vianney.leboutteiller@cea.fr; vianney@isc.astro.cornell.edu

² Center for Radiophysics and Space Research, Cornell University, Space Sciences Building, Ithaca, NY 14853-6801, USA

³ Koninklijke Sterrenwacht van België, Ringlaan 3, 1180 Brussels, Belgium

⁴ Astrophysics Group, Department of Physics and Astronomy, University College London, Gower Street, London WC1E 6BT, UK

⁵ Department of Physics and Astronomy, The Johns Hopkins University, 3400 North Charles St. Baltimore, MD 21218, USA

⁶ Department of Physics, United States Naval Academy, 572C Holloway Road, Annapolis, MD 21402, USA

⁷ Department of Astronomy, University of Virginia, PO Box 400325, Charlottesville, VA 22904, USA

⁸ Institut d'Astrophysique Spatiale, CNRS/Université Paris-Sud 11, 91405 Orsay, France

⁹ Lowell Observatory, 1400 West Mars Hill Rd., Flagstaff, AZ 86001, USA

¹⁰ Sub-Department of Astrophysics, University of Oxford, Denys Wilkinson Building, Keble Road, Oxford OX1 3RH, UK

Received 24 July 2012 / Accepted 5 September 2012

ABSTRACT

Context. We report the detection of oxygen-rich circumstellar envelopes in stars of the nearby (700 kpc) starburst galaxy IC 10. The star-formation history and the chemical environment of this galaxy make it an ideal target to observe dust production by massive stars in a metal-poor environment.

Aims. The goal of this study is to identify oxygen-rich stars in IC 10 and to constrain their nature between asymptotic giant branch stars (AGBs), red supergiants (RSGs), and other bright infrared sources. We examine the mass-loss rates of the stars and compare to results obtained for the Magellanic Clouds. Our objectives are to (1) assess whether RSGs can be significant dust producers in IC 10, and (2), solve the discrepancy between the star-formation history of IC 10 and the relatively low number of RSGs detected in the optical.

Methods. We search for silicate dust in emission by using the spectral map observed with the Infrared Spectrograph on board the *Spitzer* Space Telescope. The optical (*UBVRI*) and infrared (*JHK*, *Spitzer/IRAC* and *Spitzer/MIPS*) photometry are used to assert the membership of the stars to IC 10 and distinguish between AGBs and RSGs. Radiative models are used to infer mass-loss rates and stellar luminosities.

Results. The luminosity and colors of at least 9 silicate emission sources are consistent with stars within IC 10. Furthermore, the photometry of 2 of these sources is consistent with RSGs. We derive dust mass-loss rates similar to the values found in the Magellanic Clouds. Accounting for the sample completeness, RSGs are not important contributors to the dust mass budget in IC 10.

Key words. stars: AGB and post-AGB – stars: atmospheres – circumstellar matter – stars: mass-loss – galaxies: individual: IC 10 – supergiants

1. Introduction

Principal contributors to the dust in the interstellar medium (ISM) are thought to be low-mass asymptotic giant branch (AGB) stars, supernovae (SNe), red supergiants (RSGs), and late-type WC Wolf-Rayet stars (e.g., Gehrz 1989). AGB stars are expected to produce significant amounts of dust in the most metal-poor sources, because their evolution timescales are shorter in such environments. For metallicities as low as $1/200 Z_{\odot}$, stars might take as short as 100 Myr to evolve from the zero-age main sequence to the AGB (Ventura et al. 2002; Herwig 2004). Boyer et al. (2012) found that AGBs produce most of the dust from cool evolved stars in the metal-poor Small Magellanic Cloud (SMC, $0.2 Z_{\odot}$), but they argue that other dust sources, such as growth from existing grains, are necessary to explain the total dust mass budget. Alternatively, it is largely debated whether cosmic dust abundance can be reconciled with

SN dust (e.g., Li et al. 2008; Maiolino et al. 2004), as measurements of the dust produced by a single SN vary dramatically ($10^{-3} M_{\odot}$ up to $0.5 M_{\odot}$; e.g., Stanimirovic et al. 2005; Matsuura et al. 2011). With these considerations in mind, massive stars could be significant contributors to the ISM dust. In metal-poor galaxies, where late-type WCs are scarce, RSGs might be the dominant dust source (Massey et al. 2005; but see Boyer et al. 2012).

The detection of infrared excesses due to mass loss in the circumstellar envelopes of evolved stars within Local Group galaxies is mostly limited to low-mass carbon-rich stars ($\sim 1-2 M_{\odot}$; e.g., Sloan et al. 2012). This is due to the star-formation history of our nearest neighbor galaxies, with the lack of a recent starburst episode that would result in pronounced populations of more massive oxygen-rich stars. From an observational point of view, probing O-rich dust production in Local Group galaxies is challenging as it requires observing the silicate emission bands in the mid-infrared. Observations of such stars have therefore been limited to just the Milky Way and the Magellanic Clouds

* Appendix A is available in electronic form at <http://www.aanda.org>

with the Infrared Space Observatory (ISO; e.g., Trams et al. 1999a,b) and the *Spitzer* Space Telescope (e.g., Buchanan et al. 2009; Groenewegen et al. 2009; van Loon et al. 2010; Woods et al. 2011; Boyer et al. 2011). The great sensitivity of *Spitzer* along with matured data analysis techniques now makes it possible to study O-rich dust spectra beyond the Magellanic Clouds and in starburst galaxies.

The nearby dwarf starburst IC 10 is an ideal target to detect O-rich stars in a metal-poor environment, like what has been done for the Magellanic Clouds. IC 10 was discovered by Mayall (1935) and Hubble (1936); it is the nearest starburst galaxy known (~ 700 kpc; Kennicutt et al. 1998; Borissova et al. 2000; Hunter 2001; Kim et al. 2009). Its size and mass are comparable to the SMC while its metallicity of $12 + \log(\text{O}/\text{H}) \approx 8.26$ ($1/2.7 Z_{\odot}$ assuming the solar abundance from Asplund et al. 2009) lies between that of the Small and Large Magellanic Cloud (Garnett 1990; Lequeux et al. 1979; Richer et al. 2001; Skillman et al. 1989). The starburst nature of IC 10 was first revealed by the discovery of a large number of WR stars by Massey et al. (1992). IC 10 has experienced several episodes of extensive star formation, with the most recent ones a few 10 s to 100 s of Myr ago (Vacca et al. 2007). The presence of a widespread population of WR stars (Massey et al. 1992; Massey & Holmes 2002; Royer et al. 2001) suggests that the IC 10 starburst is also widespread and that RSGs are to be expected throughout the galaxy. At low metallicities, the number of RSGs should even dominate over the number of WR stars, as one expects from evolutionary theory (Maeder et al. 1980) and as demonstrated observationally in the Local Group by Massey (2002, 2003). The number of spectroscopically confirmed WRs in IC 10 is 24, and the actual number is believed to be many more (Massey & Holmes 2002). From the relatively low metallicity of IC 10, one would thus expect the population of RSGs to be about 50–100 (see Fig. 12 of Massey 2003), which is consistent with the color–magnitude diagram (CMD) of this galaxy.

After presenting the observations in Sect. 2, we derive a preliminary silicate emission map of IC 10 from which we identify several O-rich candidates (Sect. 3). We then cross-correlate our sample with optical and infrared catalogs, removing foreground stars in the process (Sect. 4). The mid-infrared spectra (Sect. 5) are used to derive mass-loss rates and discuss the stellar chemistry of the sources (Sect. 6).

2. Observations

IC 10 was observed with the Infrared Spectrograph (IRS; Houck et al. 2004) onboard *Spitzer* (Werner et al. 2004) on 2008 September 13 as part of GTO program 50318. Observations consisted of a sparse spectral map with the Short-Low (SL) module, providing wavelength coverage between ≈ 5 – $14.5 \mu\text{m}$ with a spectral resolution $\lambda/\Delta\lambda$ between 60 and 130. The map is made of 58 perpendicular steps and 8 parallel steps, with 2 cycles of 14 s per exposure. The galaxy was not fully sampled spatially because of time constraints. A gap was deliberately introduced between every perpendicular scanning position, with the gap size precisely equal to the width of the SL aperture ($\approx 3.7''$). The full width at half maximum (FWHM) of the point spread function is on the order of the aperture width ($\approx 3.5''$ at $10 \mu\text{m}$), allowing the detection of light from outside the slit despite the gaps.

The flux is calibrated by performing optimal extraction of the point-like sources and accounting for the slit throughput (Sect. 5). In order to solve the incomplete spatial sampling for the preliminary analysis (Sect. 3), gaps were interpolated using

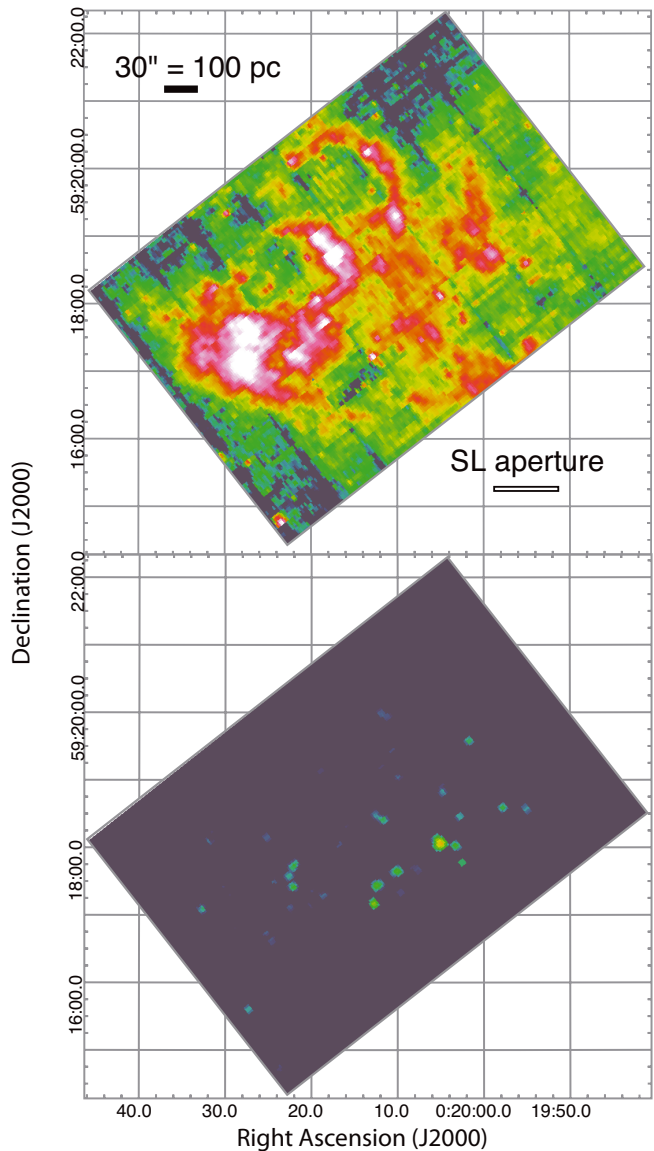


Fig. 1. *Spitzer*/IRS map. The top panel shows the distribution of the flux integrated from 7.4 to $14.5 \mu\text{m}$. The effective spatial resolution of the map ($\approx 3.2''$) is approximately equal to the width of the SL aperture. The silicate strength map is presented in the bottom panel (Sect. 3).

a cubic spline over 2 pixels on each side. We estimate the effective spatial resolution of the map to be somewhat larger than the resolution at $14.0 \mu\text{m}$, i.e., $\text{FWHM} \approx 1.8 \text{ px} = 3.7''$.

A preliminary automatic cleaning of each exposure was performed using IRSCLEAN¹. The data were then imported and analyzed with CUBISM (version 1.7; Smith et al. 2007). A second manual cleaning step was performed using the backtracking tool provided by CUBISM. Several exposures at the edges of the map were chosen to remove the background emission, which mostly arises from the Milky Way. Images corresponding to relevant wavelength ranges for building the silicate strength map (Sect. 3) were extracted with CUBISM. Figure 1 shows the map of the integrated flux in the mid-IR range.

Near-infrared photometry of stars toward IC 10 is taken from the 2MASS point-like source catalog (Skrutskie et al. 2006) while optical photometry is taken from the Local Group

¹ Version 1.9;

<http://irsa.ipac.caltech.edu/data/SPITZER/docs/>

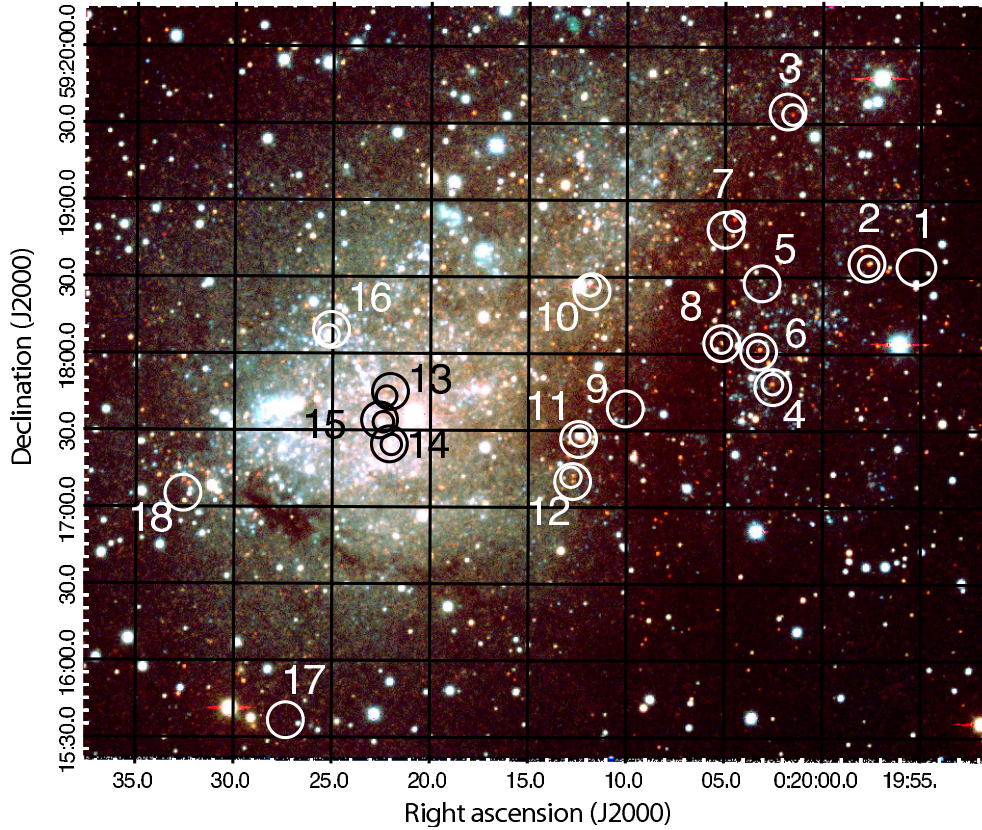


Fig. 2. Optical image of IC 10, with *I*, *B*, and *V* band images as RGB colors. The outer circles (7'' radius; ≈ 24 pc) are centered on the point-like sources with silicate emission (Table 1). The inner circles (4'' radius; ≈ 14 pc) indicate the position of the 2MASS counterpart (Table 2). The size of the circles is chosen just for display purposes. The IRS spectra are extracted from a beam with $FWHM \approx 4''$.

Galaxies Survey (LGGs; Massey et al. 2007). In addition, we measured the mid-IR photometry using the Infrared Array Camera onboard *Spitzer* (IRAC; Fazio et al. 2004) and the Multiband Imaging Photometer for *Spitzer* (MIPS; Rieke et al. 2004). IC 10 was observed with IRAC on 2004 July 23 with the 4 channels, centered respectively at 3.6, 4.5, 5.8, and 8.0 μm (AOR key 4424960), and with MIPS on 2004 December 26 at 24 μm , 70 μm , and 160 μm (AOR key 4425472). Point-like sources were identified with the software MOPEX² in all IRAC bands and in the MIPS 24 μm band.

The longer wavelength bands of MIPS were not used because of the low spatial resolution. Similarly, we did not use data from the Wide-Field Infrared Survey Explorer (WISE; Wright et al. 2010) at 3.4, 4.6, 12, and 22 μm , because of the coarser spatial resolution (from 6.1'' to 12'') as compared to IRAC (1.66–1.98'') and MIPS 24 μm (6'').

The low Galactic latitude of IC 10 (-3.34°) results in a high extinction, $E(B - V) = 0.81$ (Massey & Armandroff 1995; Massey et al. 2007), reddening the observations significantly, even in the near-IR. Using the value of $E(B - V) = 0.81$, and assuming the total-to-selective extinction ratio $R_V = 3.05$, we de-reddened the *UBVR* observations following the prescription of Table 3.21 in Binney & Merrifield (1998). Magnitudes from the *I* band to the IRAC 8.0 μm band were corrected for extinction using the power law prescription of Martin & Whittet (1990), summarized by Glass (1999).

3. Pixel-based analysis

In order to identify dust-enshrouded O-rich stars in IC 10, a silicate-strength map was built from the IRS map (Sect. 2). Silicate dust is searched for in emission via the 9.7 μm emission feature, which originates from the Si–O bond stretching mode (e.g., Knacke & Thomson 1973). Following Spoon et al. (2007), the silicate strength S_{sil} is defined as:

$$S_{\text{sil}} = \ln \frac{f_{9.7,\text{obs}}}{f_{9.7,\text{cont}}}, \quad (1)$$

where $f_{9.7,\text{obs}}$ is the observed flux density at 9.7 μm , and $f_{9.7,\text{cont}}$ is the continuum flux density at the same wavelength.

We estimated $f_{9.7,\text{cont}}$ by using the continuum maps at ~ 5.4 μm (median flux within 5.2–5.6 μm) and 14.0 μm (median flux within 13.7–14.3 μm), both extracted with CUBISM. The 5.4 μm map was then degraded to reach the spatial resolution of the 14.0 μm map (3.7'') and the continuum shape was calculated by applying the spline method adapted to PAH-dominated spectra, as described by Spoon et al. (2007). Finally, we also extracted the 9.7 μm map and convolved it to a 3.7'' resolution in order to estimate $f_{9.7,\text{obs}}$. We calculated S_{sil} using Eq. (1) for all the pixels with $f_{9.7,\text{obs}} > 1$ mJy.

Figure 1 shows the resulting silicate emission map. Based on the FWHM of sources in Fig. 2, the spatial resolution ranges from 3'' to 4'', i.e., about 10–14 pc at a distance of 700 kpc. A total of 18 point-like sources were selected based on their appearance and when $S_{\text{sil}} > 0.05$ (Table 1; Fig. 2). We find no evidence of spatial clustering and no evidence of extended silicate emission.

² Version 18.3.3;
<http://ssc.spitzer.caltech.edu/postbcd/mopex.html>

Table 1. Candidate silicate emission sources.

ID	α (J2000), δ (J2000)	ID	α (J2000), δ (J2000)
#1	00:19:55.1, +59:18:34.7	#10	00:20:11.8, +59:18:25.5
#2	00:19:57.8, +59:18:36.6	#11	00:20:12.4, +59:17:26.3
#3	00:20:01.8, +59:19:34.9	#12	00:20:12.8, +59:17:10.6
#4	00:20:02.6, +59:17:46.6	#13	00:20:22.1, +59:17:43.9
#5	00:20:02.9, +59:18:27.3	#14	00:20:22.1, +59:17:24.9
#6	00:20:03.5, +59:18:01.4	#15	00:20:22.6, +59:17:34.6
#7	00:20:04.5, +59:18:50.0	#16	00:20:25.1, +59:18:08.8
#8	00:20:04.9, +59:18:03.3	#17	00:20:27.3, +59:15:37.0
#9	00:20:10.1, +59:17:39.3	#18	00:20:32.6, +59:17:05.7

We wish to emphasize that the silicate strengths inferred from the pixel-based analysis (Fig. 1) are only indicative and include systematic uncertainties. The map interpolation and the convolution to homogenize the data lead to uncertain pixel values (Sect. 2). Most importantly, significant background emission from the ISM of IC 10 prevents an accurate estimate of the silicate dust emission from the sources. Final values of the silicate strength are derived using optimal spectral extraction (Sect. 5).

It is difficult to estimate the sample completeness based on the silicate strength map alone. Given the presence of gaps in the map (Sect. 2) and given that the point spread function is slightly more extended than the SL slit height ($\approx 3.7''$), we could be missing somewhat less than half of the sources. The present sample is mostly limited by the flux at $10 \mu\text{m}$ (see also Sect. 6.3).

4. Optical and infrared counterparts

4.1. 2MASS catalog

Most candidate silicate-emission sources in Table 1 could be associated with a 2MASS source from the point-like source catalog (Table 2). Given the spatial resolution of the silicate strength map ($3''$ – $4''$; Sect. 3), we considered positive matches for association of $4''$ or less between the source centroid in the silicate strength map and the 2MASS coordinates. Most sources were matched within $2''$ or less, corresponding to about 6.8 pc in actual distance. There were no multiple matches within $4''$. We consider from now on the 2MASS coordinates as our reference coordinates for the candidate silicate-emission sources.

Sources #1, #5, #9, #17, and #18 could *not* be associated with 2MASS point-like sources. Source #18 is $4.4''$ away from 2MASS 00203222+5917091 in the extended-source catalog. Multiple sources from the LGGs (optical) catalog are seen close to this source, but no match in the IRAC $8.0 \mu\text{m}$ band was found (Sect. 4.2). For this reason, and because the coordinate match between source #18 and the 2MASS counterpart is somewhat larger than the map resolution ($\approx 4''$), we exclude this source from the following discussion. The matches between the other sources and IRAC sources are discussed in Sect. 4.2.

4.2. IRAC and MIPS sources

We cross-correlated our sample with sources identified in the IRAC maps with MOPEX (Sect. 2). At the spatial resolution of the IRAC $3.6 \mu\text{m}$ map ($1.66''$ or $\approx 5.6 \text{ pc}$), sources #4, #8, #11, and #12 appeared to be slightly elongated while sources #10 and #16 are multiple or clearly extended. Based on the radii fitted by MOPEX, the other sources are point-like. Table 3 presents the IRAC magnitudes.

Source #17 is not a 2MASS source, but it could be matched with an IRAC point-like source. It is likely to be significantly

embedded so that even the near-IR bands are extinguished by dust. Thus, we include this source in the following discussion. Sources #1, #5, and #9 are either significantly far from any IRAC source or they are part of extended emission in the IRAC bands. These 3 sources are excluded in the following discussion since they also do not have a 2MASS point-like source counterpart.

Sources #12 and, to a lesser extent, #8 and #11 are matched with MIPS $24 \mu\text{m}$ point-like sources (Fig. 3). The spatial resolution at $24 \mu\text{m}$ is $6''$ (corresponding to $\approx 20.4 \text{ pc}$), i.e., somewhat larger than the silicate strength map resolution ($\approx 3.5''$, Sect. 3). We verified that there were no multiple IRAC sources contributing to the extraction aperture at $24 \mu\text{m}$.

4.3. LGGs catalog

Matches with the optical LGGs sample were found within $\sim 1''$ of the 2MASS coordinates for all sources in our remaining sample (Table 4), except for sources #3 and #11. Because of the large IRS and IRAC beams, we consider that any LGGs sources within $\sim 4''$ could contribute to the extracted IR fluxes. Tables A.1 and A.2 list the LGGs sources found within $4''$ of the 2MASS counterpart. In practice, only sources #12, #13, #14, and #16 in our sample have several bright infrared LGGs stars within such a radius. It must be kept in mind in the following that these sources could be multiple objects.

For all the other sources, we cannot exclude that compact stellar clusters might be affected by confusion, even in the optical LGGs observations. Such clusters would have to be smaller than $\sim 1''$ ($\sim 3 \text{ pc}$) to be unresolved in the LGGs. We explored the high-spatial resolution observations from the *Hubble Space Telescope* (HST) to investigate further the possible presence of compact stellar clusters. For this test, only sources that are members of IC 10 are considered (Sect. 4.4). Only sources #3, #7, #8, #12, #13, and #14 were covered by the observations with the Advanced Camera for Surveys (ACS) (Fig. 4). There is no evidence of enhanced clustering toward these sources, except maybe for source #8, with a few bright stars within the IRS extraction aperture. In the following, we assume that the flux extracted with 2MASS, IRAC, and with the IRS is dominated by the LGGs object found closest to the 2MASS coordinates.

4.4. Field contamination by foreground stars

We now investigate the photometry of the objects associated with the candidate silicate-emission sources (Tables 2 and 4) in order to test their membership in IC 10 and their intrinsic stellar properties. As explained by Massey et al. (2007), the V magnitude and $B - V$ color provide a good diagnostic of the stellar type while also separating foreground stars from stars in IC 10. Figure 5 shows the photometric data from Massey et al. with the candidate silicate-emission sources from Table 1 overlaid. According to Massey et al., RSGs belonging to IC 10 are expected to have $B - V \geq 2$ and $V \leq 20$. Only sources #4, #6, #7, #8, #12, #13, and #14 fit these criteria. The other sources (#2, #10, and #15) could be yellow supergiants, but they are far more likely foreground stars. Note that sources #3 and #11 have no optical counterparts (Sect. 4.3). Diagnostics for these 2 sources are based on their IR photometry alone. Figure 5 also shows the LGGs sources found within the search radius of the candidate silicate-emission sources from Table A.1. Only 3 sources have optical colors expected from RSGs, but they are not the brightest infrared sources within the search radius.

Table 2. 2MASS photometric data of associated stars.

ID	2MASS ID ^a	<i>J</i>	<i>H</i>	<i>K</i>
Foreground stars				
#2	00195768+5918349 (1.9'')	(15.19)	(14.44 ± 0.06)	(13.71)
#10	00201183+5918267 (1.3'')	(13.57)	15.39 ± 0.16	14.75 ± 0.16
#11	00201237+5917279 (1.7'')	13.62 ± 0.03	12.56 ± 0.04	12.08 ± 0.03
#15	00202240+5917332 (2.0'')	15.44 ± 0.07	14.60 ± 0.06	14.02 ± 0.07
#16	00202520+5918070 (1.9'')	14.95 ± 0.08	13.96 ± 0.08	(13.18)
IC 10				
#3	00200155+5919332 (2.5'')	15.66 ± 0.08	14.60 ± 0.06	14.01 ± 0.07
#4	00200259+5917481 (1.5'')	15.23 ± 0.06	14.15 ± 0.05	13.56 ± 0.05
#6	00200322+5918013 (2.1'')	15.19 ± 0.06	14.05 ± 0.06	13.67 ± 0.06
#7	00200452+5918521 (3.6'')	15.57 ± 0.06	14.4 ± 0.07	13.79 ± 0.04
#8	00200510+5918039 (1.7'')	15.60 ± 0.08	14.81 ± 0.10	14.13 ± 0.07
#12	00201270+5917121 (1.7'')	16.06 ± 0.11	14.88 ± 0.10	14.51 ± 0.10
#13	00202225+5917432 (1.4'')	15.59 ± 0.09	14.47 ± 0.09	13.76 ± 0.07
#14	00202199+5917244 (0.9'')	14.72 ± 0.05	13.60 ± 0.05	13.24 ± 0.05

Notes. Sources #1, #5, #9, #17, and #18 could not be matched with any 2MASS sources. Magnitudes in parentheses indicate upper limits or uncertain measurements. The field stars are identified based on the color diagnostics discussed in Sect. 4.4. ^(a) The distance between the source centroid in the silicate strength map and the associated 2MASS catalog is indicated in the parentheses.

Table 3. *Spitzer* photometry.

ID	[3.6]	[4.5]	[5.8]	[8.0]	[24]
Foreground stars					
#2	13.31	...	13.01
#10 ^a	13.15
#11	11.67	11.68	11.35	10.97	8.43 ± 0.30
#15	13.64	13.55	13.57	13.15	...
#16 ^a	12.94	12.87	12.55
IC 10					
#3	13.32	... ^b	12.59	... ^b	...
#4	13.29	13.16	12.83	12.47	...
#6	13.05	13.04	12.82	12.55	...
#7	13.29	... ^b	12.98	... ^b	...
#8	13.21	12.65	12.15	11.13	7.62 ± 0.30
#12	13.74	12.96	12.23	10.77	5.90 ± 0.10
#13	13.20	...	12.40
#14	13.12	13.16	12.37
Unknown membership					
#17	14.99	13.81	12.90	12.07	...

Notes. Magnitudes calculated assuming zero-magnitude fluxes from the instrument handbooks. The uncertainties are ≈0.01, ≈0.01, ≈0.02, and ≈0.03 for [3.6], [4.5], [5.8], and [8.0] respectively. Bands with no data correspond to sources that were not found by the MOPEX algorithm to detect point sources, unless otherwise noted. Membership is based on the color diagnostics discussed in Sect. 4.4. ^(a) Blended or multiple objects. ^(b) Not covered by the IRAC observation.

For an independent test of membership, we have used the Besançon population synthesis model (Robin et al. 2003) to count the number of foreground stars expected toward IC 10 with colors and magnitudes similar to those expected from RSGs in IC 10. We used the expected *V* magnitude and *B* − *V* color of RSGs in IC 10 from Massey et al. (2007) and found that no foreground stars can, at the same time, be that red and that bright.

Finally, near-infrared photometry further constrains the membership to IC 10. Based on an offset field of view, Borissova et al. (2000) conclude that foreground stars have colors such that $0.4 \leq J - K \leq 1.0$, and $H - K \leq 0.1$. All the sources in Table 2 have $H - K > 0.1$ and $J - K$ between 1.4 and 1.8, which bolsters our confidence that sources #4, #6, #7, #8, #12, #13, and #14 belong to IC 10. Moreover, Borissova et al. estimate that RSGs

should have $J - K \sim 1.4$ and $13 \lesssim K \lesssim 15$ while AGB stars should be fainter. Source #11, which has no optical counterpart, has $K = 12.1$ and does not fit the constraints above. It is brighter in the *K* band by one order of magnitude than the other sources and is likely a foreground star. All the other sources have $1.4 < J - K < 1.8$. In particular, source #3, which also has no optical counterpart, could be a RSG in IC 10 based solely on its *JHK* colors.

In summary, both the optical and IR photometry of sources #4, #6, #7, #8, #12, #13, and #14 are consistent with membership in IC 10. Furthermore, the *K* magnitudes of these sources (and of source #3) suggest that they are RSGs. We refine the determination of the stellar nature in Sect. 6.

5. Mid-infrared spectra

In this section, we present the mid-IR *Spitzer*/IRS spectra of all the candidate silicate-emission sources. We consider sources #3, #4, #6, #7, #8, #12, #13, and #14, which are members of IC 10, as well as #17 (IRAC source).

The presence of spatially extended MIR emission (dominated by polycyclic aromatic hydrocarbon features and warm dust continuum) prevents a regular spectral extraction of the sources, which simply sums all flux within a spatial window. We therefore used the optimal extraction provided by SMART-AdOpt³ (Lebouteiller et al. 2010) to extract the spectra at the matching stellar location in the exposure images. Optimal extraction weighs the spatial profile of the source by using the instrument PSF as a reference. The extended interstellar emission in IC 10 was removed simultaneously using a second- or third-order polynomial. The stellar location within the IRS SL aperture was constrained not only in the cross-dispersion direction but also in the dispersion direction, thereby allowing us to correct for the slit throughput and to produce an accurate flux calibration. Figure 6 presents an example of extraction, while Fig. 7 presents the final spectra.

The spectral trace was detected for all the sources mentioned above. Detection levels (based on the integrated SL wavelength range) are given in Table 5. Besides the bright sources #8

³ Version 8.2.4;

<http://isc.astro.cornell.edu/IRS/SmartRelease>

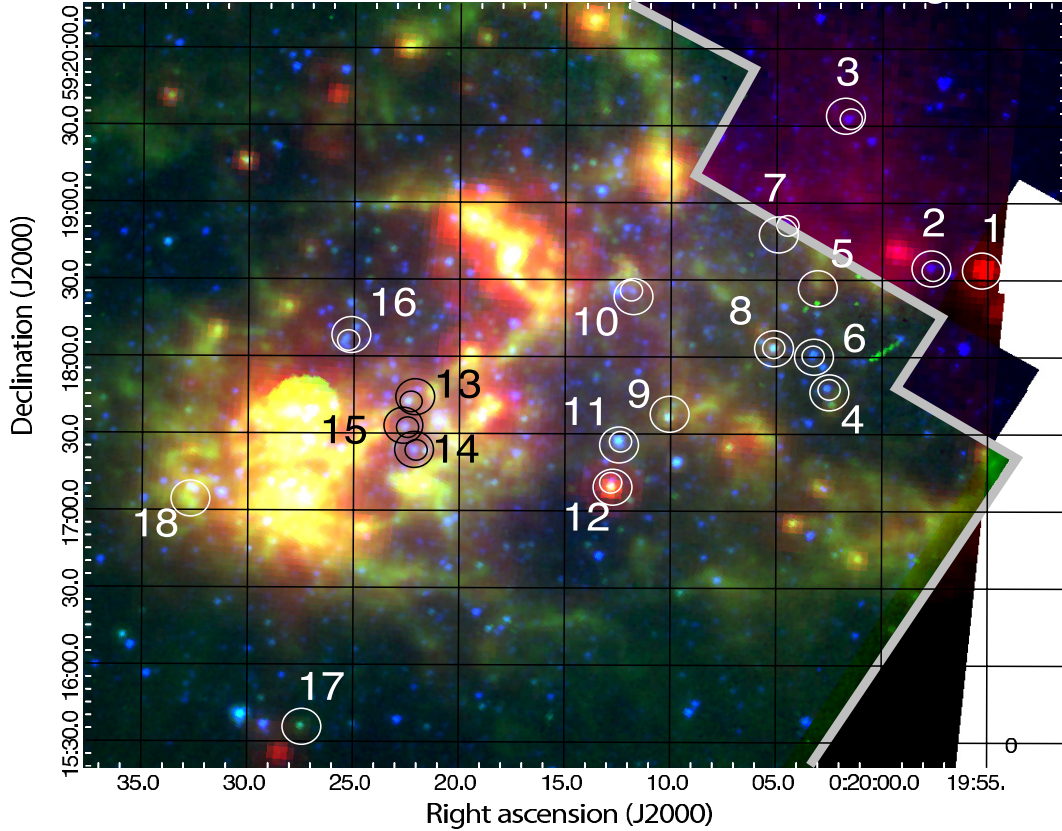


Fig. 3. *Spitzer* image (R: MIPS [24], G: IRAC [8.0], B: IRAC [3.6]). See Fig. 2 for the symbol description. Sources #8, #11, and #12 are $24\ \mu\text{m}$ point-like sources. The gray polygon shows the area covered in all bands.

Table 4. Optical photometric data of associated stars.

ID	LGGS ID ^a	<i>U</i>	<i>B</i>	<i>V</i>	<i>R</i>	<i>I</i>
Foreground stars						
#2	J001957.61+591835.5 (0.8'')	...	22.58	20.94	19.90	18.77
#10	J002011.91+591827.6 (1.0'')	21.70 ± 0.01	21.29	19.91	19.03	18.07
#11
#15	J002022.52+591732.9 (0.9'')	19.53	19.34	18.40	17.81	17.17
#16	J002025.23+591807.3 (0.5'')	19.89 ± 0.02	19.96	20.86 ± 0.06	19.45	18.50 ± 0.01
IC 10						
#3
#4	J002002.61+591748.2 (0.2'')	...	24.67 ± 0.02	21.63	19.62	17.43
#6	J002003.23+591801.6 (0.3'')	...	24.02	21.27	19.43	17.39
#7	J002004.54+591852.3 (0.2'')	...	25.29 ± 0.08	22.56 ± 0.02	20.35	17.92
#8	J002005.11+591804.1 (0.2'')	...	23.35 ± 0.02	21.10	19.43	17.71
#12	J002012.73+591712.3 (0.2'')	...	24.54 ± 0.02	22.02 ± 0.01	20.30	18.32
#13	J002022.28+591743.3 (0.2'')	...	23.92 ± 0.01	21.68 ± 0.01	19.81	17.71
#14	J002022.01+591724.5 (0.1'')	...	22.74	20.10	18.52	16.89

Notes. Errors are below 0.01 dex unless otherwise noted. The field stars are identified based on the color diagnostics discussed in Sect. 4.4. ^(a) The distance between the source centroid in the silicate-strength map and the associated LGGS catalog is indicated with parentheses. The LGGS ID gives the best match within the search radius (see Tables A.1 and A.2).

and #12, we note that sources #4, #6, #13, and #17 are fairly well detected (more than 2σ), while sources #3, #7, and #14 barely stand above the detection threshold. Based on the comparison between the source spatial profile and the IRS point spread function, we find that all sources are point-like at the spatial resolution of the IRS SL module at $10\ \mu\text{m}$, i.e., $\approx 2''$.

Sources #8 and #12 show prominent silicate emission peaking at 8 mJy, and 11 mJy respectively, while source #4 shows weak emission peaking at ≈ 3 mJy (Fig. 7). The signal-to-noise

ratio of the other sources is too low to assert unambiguously the presence of silicate dust. Table 5 gives the silicate strength values. The peak flux density of the silicate emission in RSGs of the Large Magellanic Cloud (LMC) ranges from ~ 1 Jy to ~ 3.5 Jy (Buchanan et al. 2009). Such sources would have fluxes around 4–14 mJy at the distance of IC 10, which compares well with our values. Source #12 is characterized by a bright dust continuum longward of $13\ \mu\text{m}$ which cannot be due to background extended emission, as it was removed during spectral extraction. This

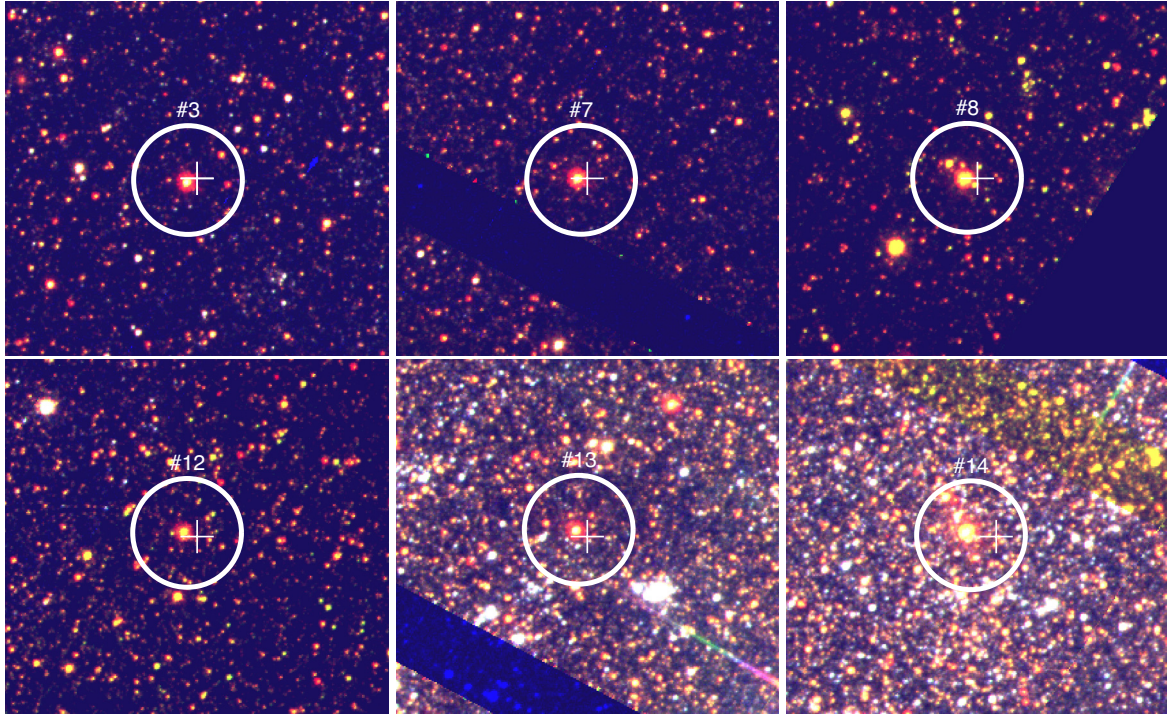


Fig. 4. HST/ACS images from candidate silicate-emission sources within IC 10. Images were downloaded from the *Hubble* Legacy Archive (<http://hla.stsci.edu/>) with *I*, *G*, and *B* band images as RGB colors. The cross indicates the 2MASS coordinates. The circle represents the size of the IRS extraction aperture, 2'' radius (corresponding to ≈ 7 pc). The other sources were not observed with ACS.

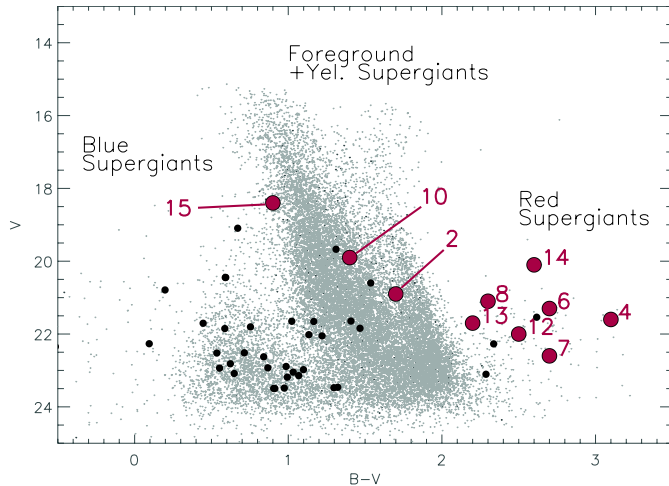


Fig. 5. *V* vs. *B*–*V* colors of stars toward IC 10 (Massey et al. 2007). Red points represent the candidate silicate-emission sources from this study. Small black points indicate LGGs sources within the search radius of the candidate silicate-emission sources (Table A.1).

object is associated with a point-like source in the MIPS 24 μ m image. The nature of the silicate emission sources is discussed in Sect. 6.1.

6. Properties of the stars

6.1. RSG vs. AGB

Several types of stars can produce silicate dust, most notably AGBs, RSGs, planetary nebulae, and novae. Young stellar objects (YSOs) also show silicate dust in their disks or outflows, although the dust grains might not be produced in situ. The

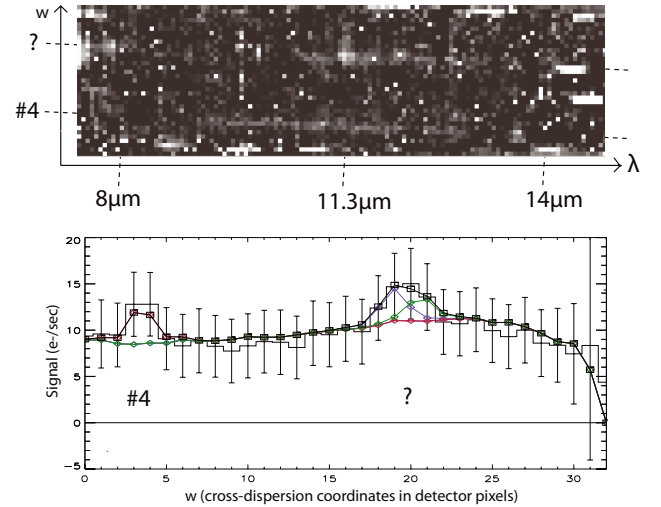


Fig. 6. Example of optimal spectral extraction (source #4). The detector image is shown in the *top panel*, after background subtraction, with the cross-dispersion profile (*w*) as a function of wavelength. The corresponding profile along the aperture (integrated signal over the wavelength range vs. *w*) is shown as a histogram in the *bottom panel*. The connected squares show the fit of the spatial components in the slit, including source #4 (red profile), the extended background emission, and another slightly extended source in IC 10 matching the location of the H II region [HL90] 17 (Hodge & Lee 1990), here fitted with 2 point-like sources showed by the green and blue profiles.

optical and near-IR colors suggest that all sources but #17 could be RSGs (Sect. 4.4). We now review this finding by comparing the K_s vs. $J - K_s$ colors of stars in IC 10 and in the LMC. Figure 8 shows the CMD in which the magnitudes of IC 10 sources have been scaled to the distance of the LMC. Sources #7 and #13 appear to fall in the O-rich AGB color domain, while source #3 lies

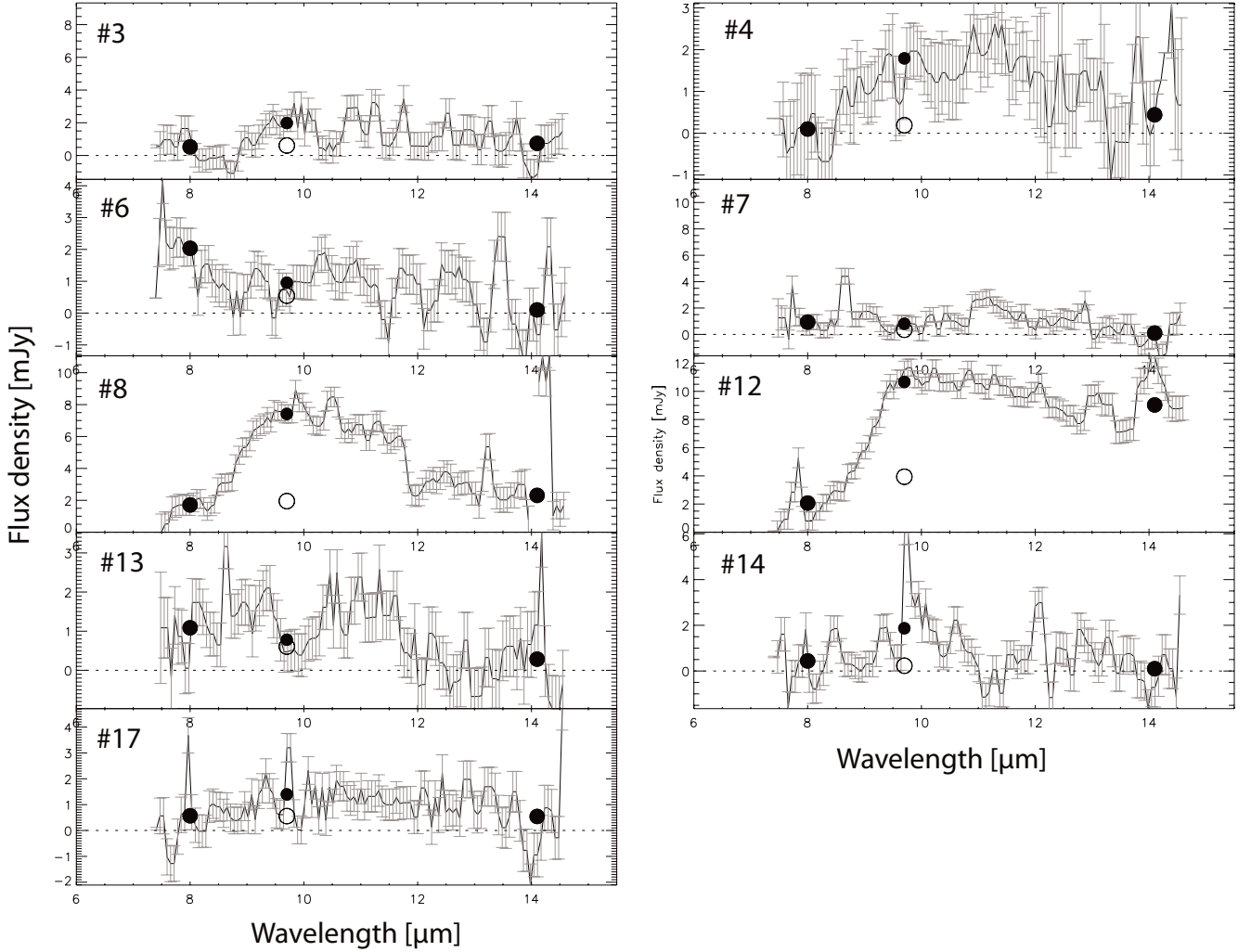


Fig. 7. *Spitzer*/IRS spectra of sources photometrically identified as members of IC 10. The 3 filled circles represent the observed continuum flux density at 8.0, 9.7, and 14.0 μm while the open circle represents the interpolated flux density at 9.7 μm used to infer the silicate strength (see text). Spectra were smoothed by a running 3-pixel median.

Table 5. Silicate strengths and model results.

ID	Detection ^a (σ)	S_{sil} (mags)	L_{bol} (L_{\odot})	T_{eff} (K)	MLR ^b ($M_{\odot} \text{ yr}^{-1}$)
#3	1.4	$+1.42^{+0.63}_{-1.47}$	120 000	3550	8×10^{-7}
#4	3.4	$+2.22^{+1.63}_{-2.15}$	130 000	3397	2×10^{-7}
#6	2.5	$-0.53^{+0.75}_{-1.64}$	130 000	3490	2×10^{-7}
#7	1.5	$-0.89^{+0.70}_{-2.34}$	110 000	3397	3×10^{-7}
#8	7.7	$+1.44^{+0.07}_{-0.07}$	120 000	3550	28×10^{-7}
#12	18	$+0.98^{+0.09}_{-0.10}$	90 000	3550	30×10^{-7}
#13	2.4	$+0.85^{+0.65}_{-2.00}$	110 000	3550	14×10^{-7}
#14	1.3	$+2.35^{+1.37}_{-2.49}$	150 000	3550	5×10^{-7}
#17	2.3	$+1.27^{+0.85}_{-3.54}$	15 000	3550	30×10^{-6}

Notes. The sources with significant silicate emission are shown in bold (Sect. 5). ^(a) Detection level over the spectral trace (integrated SL wavelength range). ^(b) Mass-loss rate determinations with a factor of ≈ 2 statistical uncertainties.

on the AGB/RSG cut. All the other sources (#2, #4, #6, #8, #12, and #14) are unlikely to be AGB stars.

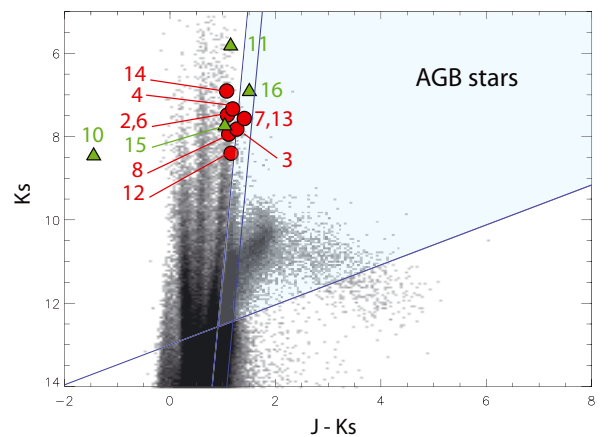


Fig. 8. K_s vs. $J - K_s$ CMD for sources in IC 10. The background is a Hess diagram of the sources from the SAGE catalog of the LMC (Meixner et al. 2006). The IC 10 sources are corrected for reddening and then “moved” to the LMC for comparison. AGB stars fall within the labeled region in the upper-right region (Cioni et al. 2006; Nikolaev & Weinberg 2000). O-rich AGB stars are redder than the left oblique line while C-rich AGB stars are redder than the right oblique line. Sources #10, #11, #15, and #16 are foreground sources not associated with IC 10, and are marked with green triangles. Source #17 is not a 2MASS source.

The most important constraint in distinguishing between AGBs and RSGs is the bolometric luminosity. It is expected that RSGs have a bolometric luminosity $M_{\text{bol}} \lesssim -7.9$ (i.e., $\gtrsim 117\,000 L_{\odot}$), while AGBs should have $M_{\text{bol}} \gtrsim -7.1$ ($\lesssim 56\,000 L_{\odot}$) (e.g., Wood et al. 1983). Although AGBs can undergo hot bottom burning or thermal pulses that can increase their brightness temporarily (e.g., Groenewegen et al. 2009), the threshold $M_{\text{bol}} \lesssim -7.9$ separates less luminous RSGs from intermediate-mass AGBs (see Massey et al. 2003; Massey & Olsen 2003). We used the MIR spectra alongside the photometry to constrain the luminosities and mass-loss rates of the sources using the radiative transfer model described by Groenewegen et al. (1995, 2009). For all stars we fitted a model with pure silicate dust (with absorption coefficients from Volk & Kwok 1988), and another one with a mixture of 20% aluminum oxide and 80% silicates. For #8 and #12 the pure silicate dust model provided the best fit, while either model fits the data for the other sources. Table 5 and Fig. 9 shows the results for the silicate dust model. Based on the model results, most of the sources are much too bright to be AGBs. Only sources #12 and #17 fall below the luminosity threshold. Sources #3, #4, #6, #7, #8, #13, and #14 are thus again compatible with RSGs.

The specific case of source #12 is puzzling, as it shows strong silicate emission, a dust continuum longwards of $10 \mu\text{m}$ which is visible in the IRS spectrum, and is detected in the MIPS $24 \mu\text{m}$ image. The *Herschel*/PACS observations (S. Madden, priv. comm.) place strict upper limits on the dust emission at far-infrared wavelengths. Due to the presence of a dust continuum, we compared the spectrum of this source to radiative transfer models of dusty young star clusters (Whelan et al. 2011). If source #12 is a young stellar cluster, then the near-IR measurements could arise from the main-sequence stars in the cluster while the long-wavelength continuum would arise from dust heated in the intra-cluster medium by the young stars. However, no models fit the data: the $24 \mu\text{m}$ flux density and the PACS upper limits were much lower than expected for a range of appropriate dust geometries, from optically thin and geometrically thick to optically thin and geometrically thin. This suggests the lack of a carbonaceous grain dust component as one would expect in a dusty star-forming environment. This finding is compatible with the lack of a clustering around source #12 in the HST images (Fig. 4). We therefore tentatively conclude that source #12 is not a young compact cluster but is an evolved dust-producing star of some kind. The silicate emission feature, low dust continuum, and relatively low luminosity (compared to RSGs) in the planetary nebula NGC 6804 suggests that source #12 may be a planetary nebula around an O-star (Bilikova et al. 2012; Weidmann & Gamen 2011), or a dusty WR star. The shallow long-wavelength spectral energy distribution (SED) is also reminiscent of extreme-AGB stars, which are usually carbon-rich (see Boyer et al. 2012, and references therein).

6.2. Mass-loss rates

Although it is possible to infer the mass-loss rate from molecular infrared transitions (e.g., Matsuura et al. 2006), the dust emission associated with the circumstellar envelope is a better tracer of mass loss. The mass-loss efficiency in O-rich stars depends more on metallicity than in C-rich stars, because O-rich dust depends on metallicity-limited elements (Si, Al), while amorphous carbon depends on self-produced C (e.g., Sloan et al. 2008, 2012).

The dust-production rate was computed from our models (Sect. 6.1), assuming an outflow velocity of 10 km s^{-1} . The total mass-loss rate is estimated using a standard gas-to-dust ratio

of 200. The mass-loss rates we infer (Table 5) lie within the range of rates found for the RSGs in the SMC and LMC, with rates between $10^{-5.5} M_{\odot} \text{ yr}^{-1}$ and $10^{-7} M_{\odot} \text{ yr}^{-1}$ (Groenewegen et al. 2009, assuming identical values for the outflow velocities and gas-to-dust ratio).

6.3. Spatial distribution and sample completeness

A comparison of the luminosities of the RSG candidates (Table 5) and theoretical isochrones (Fagotto et al. 1994) suggests that the silicate-emission sources in our sample (all but #17) are more massive than $\gtrsim 12 M_{\odot}$. Their expected lifetime is $\sim 20 \text{ Myr}$ old, which is consistent with a starburst population. Is the spatial distribution of the RSG candidates compatible with the starbursting region? The claim for a starburst in IC 10 mainly originates from the discovery of over 100 WR stars (Massey et al. 1992; Royer et al. 2001; Massey & Holmes 2002). These studies showed that the spatial distribution of the WR stars is quite uniform, suggesting a widespread starburst. Hence, we do not expect to find the RSGs in any particular region, which is supported by our results.

We expect the number of RSGs to dominate the number of WR stars at low metallicity, with a lower limit of 50 RSGs in IC 10 (e.g., Maeder et al. 1980; Massey et al. 2002, 2003). Our current sample sets a lower limit on the actual number of O-rich dust-enshrouded stars and RSG candidates, with notably a strong limitation by the *Spitzer*/IRS sensitivity at $10 \mu\text{m}$. In order to quantify the completeness of the sample, we build a sample of stars with similar colors as the RSG candidates we already identified. Following Sects. 4.4 and 6.1, we choose the following constraints: $J - K = 1.5 \pm 0.2$, $H - K > 0.3$, $B - V > 2.2$, and $V - R > 1.6$. Only 16 sources in the 2MASS/IRAC cross-matched sample (633 stars) fit these constraints, including the already confirmed sources #4, #8, and #12 (Table 6). None of the other 13 sources show silicate emission in their IRS spectra. We partly attribute this low number of silicate-emission sources to the low signal-to-noise ratio in the IRS spectra, as indicated by the IRAC $8 \mu\text{m}$ magnitudes. Only one source, 2MASS 00200459+5918198, is expected to be bright enough for the silicate emission to be detected, and its $[5.8] - [8.0]$ color does suggest the possible presence of silicate emission. However, the $8 \mu\text{m}$ flux is likely to be overestimated due to contamination by PAH emission which might not have been completely subtracted when performing the aperture photometry with a sky annulus. In addition to the 3 sources we already identified as RSGs, 13 more could thus also be RSGs. Considering an average mass-loss rate of $5 \times 10^{-7} M_{\odot} \text{ yr}^{-1}$ (Sect. 6.2), this results in a total mass-loss rate of $8 \times 10^{-6} M_{\odot} \text{ yr}^{-1}$ for IC 10 (see discussion in Sect. 6.4).

The low number of RSGs was already noticed by Massey et al. (2007), using deep optical images (photometry uncertainties of 0.004 in V and 0.015 in B for $B = 24.3$) and better spatial resolution than 2MASS and *Spitzer* observations. They argue that a very recent burst ($\lesssim 10 \text{ Myr}$) could produce the large WR/RSG population ratio. Although our *Spitzer* data uncover just the tip of the RSG iceberg, the missing RSGs in IC 10 remain a mystery.

6.4. Discussion

Our analysis of stellar properties shows that the luminosities of red supergiants in IC 10 are above $90\,000 L_{\odot}$ (Table 7). Stellar evolution models show that stars with an initial mass higher

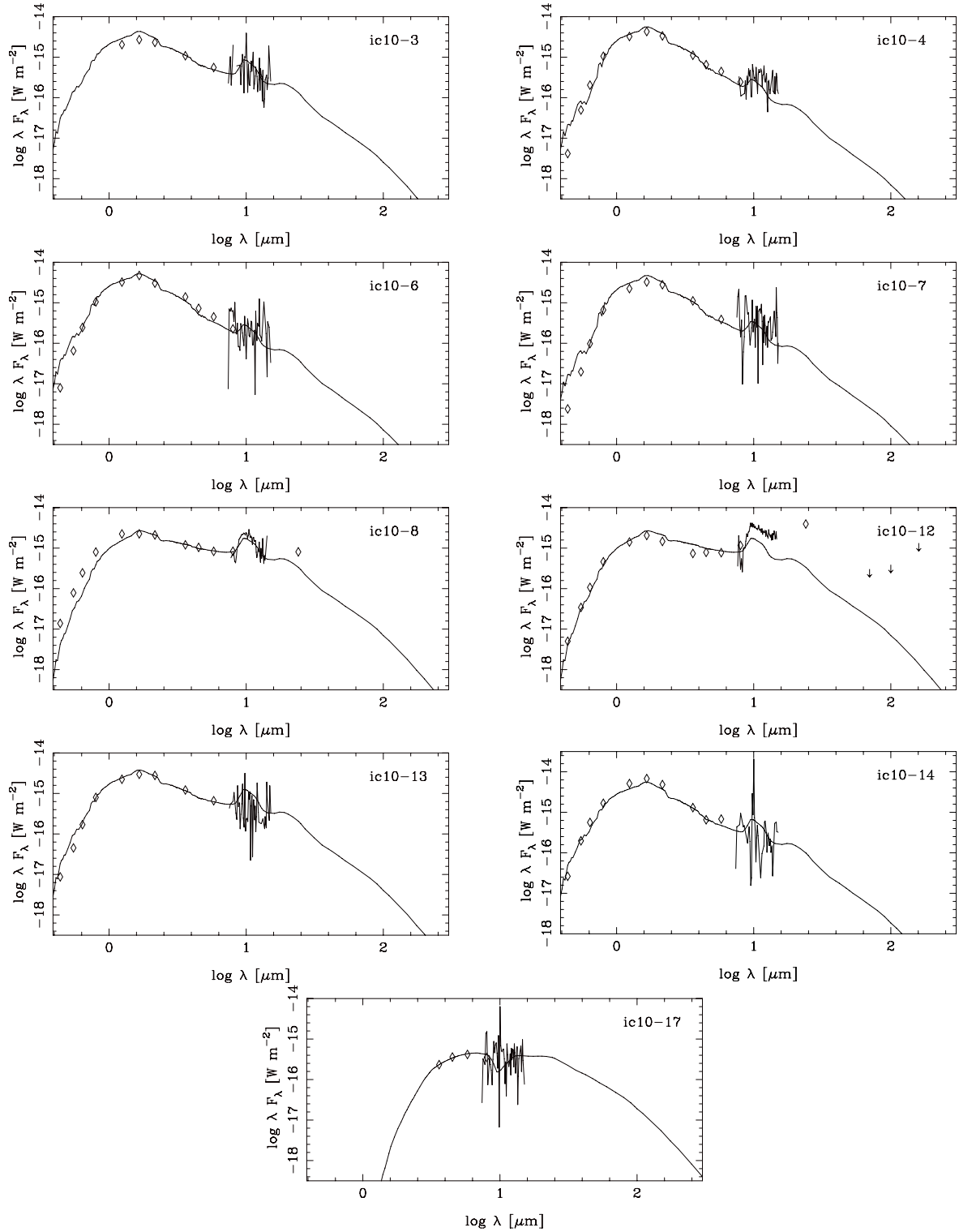


Fig. 9. SED fit results. For each source, the SED model is shown on top as the solid curve, with the diamonds indicating photometry points from the optical bands, 2MASS, and *Spitzer*, and with the segments indicating the IRS data. The [24] data point for source #8 bears significant uncertainties (see Table 3). The downward arrows for source #12 show the upper limits on the *Herschel*/PACS fluxes. Source #12 could not be fitted by our models (Sect. 6.1).

than $11.7 M_\odot$ can reach luminosities higher than $90\,000 L_\odot$ during the RSG phase (Fagotto et al. 1994). Stars lower than $9 M_\odot$ mass cannot reach such a high luminosity, though the calculated mass range lacks $9\text{--}11.7 M_\odot$ stars, which evolve into the super-AGB phase. The models further predict that the age to reach such high luminosities is about 20 Myr old or younger.

The age of RSGs is consistent with the star-formation history of this galaxy. Hunter (2001) analyzed stellar clusters and uncovered several episodes of high star-formation. Resulting components include young clusters (4–30 Myr), presumably formed in the starbursts, and intermediate age clusters (450 Myr). The age of the RSGs corresponds to the starburst phase of this galaxy and

Table 6. Sources with colors similar to confirmed silicate emission sources.

2MASS source	K	[8.0]	[5.8]–[8.0]
00201538+5919070	13.52
00200259+5917481 (#4)	13.57	12.47	0.36
00200322+5918013	13.67	12.55	0.27
00202465+5919003	13.92
00203019+5917154	14
00200459+5918198	14.09	12.45	0.78
00200510+5918039 (#8)	14.13	11.13	1.02
00200825+5919092	14.26
00200277+5917564	14.28	13.21	0.21
00202179+5917477	14.36
00195375+5918118	14.43
00202036+5918205	14.51
00200839+5916419	14.51	14.07	0.41
00201270+5917121 (#12)	14.51	10.77	1.46
00200848+5916552	14.76	13.65	0.37
00200819+5919202	15.06

Notes. Constraints on the colors are $J - K = 1.5 \pm 0.2$, $H - K > 0.3$, $B - V > 2.2$, and $V - R > 1.6$.

it is consistent with the large population of WR stars detected by (Massey & Holmes 2002).

Our analysis might provide a unique case of measuring mass-loss rates of such young red supergiants. RSGs in IC 10 might result from recent starbursts (4–30 Myr), while RSGs in the LMC are mostly from intermediate age clusters (a few 100 s of Myr; Elson & Fall 1988; van Loon et al. 1999). The mass-loss rates of young RSGs are typically 10^{-7} – $10^{-6} M_{\odot} \text{ yr}^{-1}$, which are comparable to those observed in LMC RSGs. We did not detect mass-loss rates higher than $10^{-6} M_{\odot} \text{ yr}^{-1}$ in our sample of RSGs (discounting #17), although such higher mass-loss rates have been found in Galactic RSGs (e.g., VY CMA with $10^{-4} M_{\odot} \text{ yr}^{-1}$; Decin et al. 2006). This might be due to the fact that our selection of RSGs is limited by the detection limit of the 2MASS photometry, where RSGs with high mass-loss rates are faint at near-IR wavelengths.

The current analysis of mass-loss rates shows that gas ejected from the RSG population into the ISM is at least $10^{-5} M_{\odot} \text{ yr}^{-1}$, and the dust return from RSGs is at least $5 \times 10^{-8} M_{\odot} \text{ yr}^{-1}$. We consider this to be a lower limit, since our project missed stars with high mass-loss rates because dust extinction in the K band prevented their detection by 2MASS. These dusty stars could contribute a significant fraction of the dust and gas produced by the RSGs in IC 10. Compared with the gas mass of IC 10 ($\sim 10^8 M_{\odot}$, Yin et al. 2010) and a star-formation rate of up to $0.2 M_{\odot} \text{ yr}^{-1}$ (Leroy et al. 2006), which represents the interstellar gas mass consumed by the formation of stars, the mass injected from RSGs is significantly small, and has little impact on the total gas ISM mass at the current stage. Although the total mass of ISM dust in this galaxy is unknown, it is likely to be on the order of $10^6 M_{\odot}$, considering the gas-to-dust mass ratio. The dust from RSGs does not appear to be an important contributor to the dust mass in this galaxy if the starbursts in the past few Myr have had similar strengths. A similar conclusion was reached for the Magellanic Clouds where AGB stars dominate the measurable stellar dust production (e.g., Boyer et al. 2012). We conclude that although RSGs could in principle dominate the dust production over AGBs in a starburst galaxy (e.g., Massey et al. 2005), this is not observed in IC 10.

7. Conclusions

We report the discovery of O-rich dust-enshrouded stars within the nearby (≈ 700 kpc) dwarf starburst galaxy IC 10. We examined the *Spitzer*/IRS spectral map (7.5–14.5 μm) in order to search for point-like sources showing silicate dust in emission. The silicate-strength map we constructed reveals several point-like sources and no extended emission.

Most sources are associated with single, point-like, 2MASS and optical sources. We investigate the colors and magnitudes in the near-IR and optical, and identify 9 sources belonging to the IC 10 system. The colors and photometry in the optical and near-infrared suggest that these sources are distinct from AGB stars. Modeling of the dust results in high luminosities compatible with RSGs. Thus, we have spectroscopically confirmed O-rich circumstellar dust at greater distances than any previous study. The low number of sources discovered spectroscopically does not solve the problem of the apparent lack of RSGs as compared to WR stars in IC 10 (Massey et al. 2007).

We derived mass-loss rates for all sources using a radiative transfer model. Accounting for sample completeness, the total dust-production rates are too small to account for the dust mass of IC 10. Other sources of dust (AGBs, SNe, WR) are necessary to explain the dust mass observed in the ISM of IC 10.

Another source (#12) belonging to the IC 10 system shows strong silicate emission together with a warm carbonaceous dust grain continuum. The nature of this source remains unknown.

Acknowledgements. We thank the anonymous referee for a helpful report. This work is based on observations made with the *Spitzer* Space Telescope, which is operated by the Jet Propulsion Laboratory, California Institute of Technology under a contract with NASA. This study made use of the Two Micron All Sky Survey (2MASS; Skrutskie et al. 2006). J.B.S. wishes to acknowledge the support from a Marie Curie Intra-European Fellowship within the 7th European Community Framework Program under project number 272820. P.M.'s contributions to this project were supported by the National Science Foundation under grant AST-1008020.

References

- Asplund, M., Grevesse, N., Sauval, A. J., & Scott, P. 2009, *ARA&A*, 47, 481
- Binney, J., & Merrifield, M. 1998, *Galactic astronomy* (Princeton, NJ: Princeton University Press)
- Bilíková, J., Chu, Y.-H., Gruendl, R. A., Su, K. Y. L., & De Marco, O. 2012, *ApJS*, 200, 3
- Borissova, J., Georgiev, L., Rosado, M., et al. 2000, *A&A*, 363, 130
- Boyer, M. L., Srinivasan, S., van Loon, J. T., et al. 2011, *AJ*, 142, 103
- Boyer, M. L., Srinivasan, S., Riebel, D., et al. 2012, *ApJ*, 748, 40
- Buchanan, C. L., Kastner, J. H., Hrivnak, B. J., & Sahai, R. 2009, *AJ*, 138, 1597
- Cioni, M.-R. L., Girardi, L., Marigo, P., & Habing, H. J. 2006, *A&A*, 448, 77
- Decin, L., Hony, S., de Koter, A., et al. 2006, *A&A*, 456, 549
- Demers, S., Battinelli, P., & Letarte, B. 2004, *A&A*, 424, 125
- Elson, R. A., & Fall, S. M. 1988, *AJ*, 96, 1383
- Fagotto, F., Bressan, A., Bertelli, G., & Chiosi, C. 1994, *A&AS*, 105, 29
- Fazio, G. G., Hora, J. L., Allen, L. E., et al. 2004, *ApJS*, 154, 10
- Garnett, D. R. 1990, *ApJ*, 363, 142
- Gehrz, R. 1989, *Interstellar Dust*, 135, 445
- Glass, I. S. 1999, *Handbook of Infrared Astronomy* (Cambridge University Press)
- Groenewegen, M. A. T. 1995, *A&A*, 293, 46
- Groenewegen, M. A. T., Sloan, G. C., Soszyński, I., & Petersen, E. A. 2009, *A&A*, 506, 1277
- Herwig, F. 2004, *ApJS*, 155, 651
- Hodge, P., & Lee, M. G. 1990, *PASP*, 102, 26
- Houck, J. R., Charmandaris, V., Brandl, B. R., et al. 2004, *ApJS*, 154, 211
- Hubble, E. P. 1936, *Realm of the Nebulae* (New Haven: Yale University Press)
- Hunter, D. A. 2001, *ApJ*, 559, 225
- Kennicutt, R. C., Jr., Stetson, P. B., Saha, A., et al. 1998, *ApJ*, 498, 181
- Kessler, M. F., Steinz, J. A., Anderegg, M. E., et al. 1996, *A&A*, 315, L27
- Kim, M., Kim, E., Hwang, N., et al. 2009, *ApJ*, 703, 816
- Knacke, R. F., & Thomson, R. K. 1973, *PASP*, 85, 341
- Lebouteiller, V., Bernard-Salas, J., Sloan, G. C., & Barry, D. J. 2010, *PASP*, 122, 231

- Lequeux, J., Peimbert, M., Rayo, J. F., Serrano, A., & Torres-Peimbert, S. 1979, A&A, 80, 155
- Leroy, A., Bolatto, A., Walter, F., & Blitz, L. 2006, ApJ, 643, 825
- Li, Y., Hopkins, P. F., Hernquist, L., et al. 2008, ApJ, 678, 41
- Maeder, A., Lequeux, J., & Azzopardi, M. 1980, A&A, 90, L17
- Maiolino, R., Schneider, R., Oliva, E., et al. 2004, Nature, 431, 533
- Martin, P. G., & Whittet, D. C. B. 1990, ApJ, 357, 113
- Massey, P. 2002, ApJS, 141, 81
- Massey, P. 2003, ARA&A, 41, 15
- Massey, P., & Armandroff, T. E. 1995, AJ, 109, 2470
- Massey, P., & Holmes, S. 2002, ApJ, 580, L35
- Massey, P., & Olsen, K. A. G. 2003, AJ, 126, 2867
- Massey, P., Armandroff, T. E., & Conti, P. S. 1992, AJ, 103, 1159
- Massey, P., Plez, B., Levesque, E. M., et al. 2005, ApJ, 634, 1286
- Massey, P., Olsen, K. A. G., Hodge, P. W., et al. 2007, AJ, 133, 2393
- Matsuura, M., Wood, P. R., Sloan, G. C., et al. 2006, MNRAS, 371, 415
- Matsuura, M., Dwek, E., Meixner, M., et al. 2011, Science, 333, 1258
- Mayall, N. U. 1935, PASP, 47, 317
- Meixner, M., Gordon, K. D., Indebetouw, R., et al. 2006, AJ, 132, 2268
- Nikolaev, S., & Weinberg, M. D. 2000, ApJ, 542, 804
- Richer, M. G., Bullesos, A., Borissova, J., et al. 2001, A&A, 370, 34
- Riebel, D., Srinivasan, S., Sargent, B., & Meixner, M. 2012, ApJ, 753, 71
- Rieke, G. H., Young, E. T., Engelbracht, C. W., et al. 2004, ApJS, 154, 25
- Robin, A. C., Reylé, C., Derrière, S., & Picaud, S. 2003, A&A, 409, 523
- Robitaille, T. P., Whitney, B. A., Indebetouw, R., Wood, K., & Denzmore, P. 2006, ApJS, 167, 256
- Robitaille, T. P., Whitney, B. A., Indebetouw, R., & Wood, K. 2007, ApJS, 169, 328
- Royer, P., Smartt, S. J., Manfroid, J., & Vreux, J.-M. 2001, A&A, 366, L1
- Skillman, E. D., Kennicutt, R. C., & Hodge, P. W. 1989, ApJ, 347, 875
- Skrutskie, M. F., Cutri, R. M., Stiening, R., et al. 2006, AJ, 131, 1163
- Sloan, G. C., Kraemer, K. E., Wood, P. R., et al. 2008, ApJ, 686, 1056
- Sloan, G. C., Matsuura, M., Lagadec, E., et al. 2012, ApJ, 752, 140
- Smith, J. D. T., Armus, L., Dale, D. A., et al. 2007, PASP, 119, 1133
- Spoon, H. W. W., Marshall, J. A., Houck, J. R., et al. 2007, ApJ, 654, L49
- Trams, N. R., van Loon, J. Th., Waters, L. B. F. M., et al. 1999a, A&A, 346, 843
- Trams, N. R., van Loon, J. Th., Zijlstra, A. A., et al. 1999b, A&A, 344, L17
- Vacca, W. D., Sheehy, C. D., & Graham, J. R. 2007, ApJ, 662, 272
- van Loon, J. T., Groenewegen, M. A. T., de Koter, A., et al. 1999, A&A, 351, 559
- van Loon, J. T., Oliveira, J. M., Gordon, K. D., Sloan, G. C., & Engelbracht, C. W. 2010, AJ, 139, 1553
- Ventura, P., D'Antona, F., & Mazzitelli, I. 2002, A&A, 393, 215
- Volk, K., & Kwok, S. 1988, ApJ, 331, 435
- Weidmann, W. A., & Gamen, R. 2011, A&A, 526, A6
- Werner, M. W., Roellig, T. L., Low, F. J., et al. 2004, ApJS, 154, 1
- Whelan, D. G., Johnson, K. E., Whitney, B. A., Indebetouw, R., & Wood, K. 2011, ApJ, 729, 111
- Wood, P. R., Bessell, M. S., & Fox, M. W. 1983, ApJ, 272, 99
- Woods, P. M., Oliveira, J. M., Kemper, F., et al. 2011, MNRAS, 411, 1597
- Wright, E. L., Eisenhardt, P. R. M., Mainzer, A. K., et al. 2010, AJ, 140, 1868
- Yin, J., Magrini, L., Matteucci, F., et al. 2010, A&A, 520, A55

Table A.1. LGGs sources within $d < 4''$ of the silicate emission candidates identified as members of IC 10.

ID	d (")	LGGs	V	$V - R$	$R - I$
#3	2.33	J002001.84+591933.9	23.463	0.684	...
	2.89	J002001.22+591934.6	22.928	0.647	1.032
	3.40	J002001.82+591930.5	22.891	0.691	0.653
	3.83	J002001.96+591935.4	23.475	1.025	0.904
#4	0.18	J002002.61+591748.2	21.629	2.008	2.192
	2.22	J002002.55+591750.3	23.484	1.020	1.241
	3.29	J002002.94+591746.2	21.804	0.492	0.480
	3.79	J002003.05+591749.5	22.522	0.440	...
#6	0.31	J002003.23+591801.6	21.274	1.848	2.035
	2.27	J002003.48+591800.2	23.084	0.537	...
	2.59	J002003.31+591803.8	23.142	0.938	1.183
	3.77	J002002.94+591804.4	21.656	0.745	0.848
#7	0.25	J002004.54+591852.3	22.559	2.207	2.428
	3.91	J002003.25+591805.2	23.494	0.703	...
#8	0.21	J002005.11+591804.1	21.096	1.666	1.717
	0.98	J002005.19+591804.6	21.529	0.238	1.206
	2.52	J002005.00+591806.3	22.979	0.720	0.601
	3.60	J002005.45+591801.5	19.672	0.875	0.997
#12	0.30	J002012.73+591712.3	22.020	1.722	1.978
	2.23	J002012.75+591709.9	22.271	1.535	1.453
	2.51	J002013.00+591713.1	23.496	0.845	1.139
	3.02	J002012.59+591715.0	22.626	0.689	1.024
	3.64	J002012.90+591715.4	23.185	0.928	1.220
	3.82	J002013.19+591711.4	21.644	0.909	0.976
#13	0.25	J002022.28+591743.3	21.682	1.870	2.095
	1.54	J002022.45+591743.0	22.817	0.632	...
	2.49	J002022.46+591741.3	21.704	0.358	0.290
	2.93	J002021.97+591741.2	20.790	0.492	0.141
	3.30	J002022.23+591746.5	22.346	2.662	1.090
	3.33	J002022.13+591746.4	20.599	1.013	0.972
	3.39	J002022.68+591742.4	21.850	0.478	0.779
	3.59	J002021.87+591741.1	19.094	0.452	0.447
#14	0.18	J002022.01+591724.5	20.096	1.581	1.626
	0.84	J002022.05+591725.1	22.266	3.631	1.774
	1.63	J002022.10+591725.8	21.842	1.368	0.601
	1.76	J002022.11+591725.9	22.051	1.566	0.616
	1.89	J002021.78+591725.4	22.936	0.132	...
	2.25	J002022.22+591723.0	23.046	1.235	1.264
	2.35	J002022.05+591722.1	21.650	0.932	1.078
	2.45	J002021.85+591722.2	22.018	0.846	1.099
	2.82	J002021.82+591726.9	23.105	1.172	1.418
	3.75	J002021.68+591721.5	20.448	0.514	0.444
3.94	J002022.44+591726.3	22.516	0.469	0.702	
3.96	J002021.60+591721.8	20.446	0.512	0.444	

Notes. The LGGs ID in bold indicates the best match in terms of distance and infrared brightness.

Appendix A: Cross-correlation LGGs stars – silicate emission candidates

The silicate emission candidates from Table 1 are matched with optical sources from the LGGs in Sect. 4.3. When several

Table A.2. LGGs sources within $d < 4''$ of the silicate emission candidates identified as field stars.

ID	d (")	LGGs	V	$V - R$	$R - I$
#2	0.80	J001957.61+591835.5	20.938	1.036	1.132
	3.12	J001957.83+591837.8	23.890	0.997	1.084
	3.49	J001957.24+591835.8	22.182	1.589	1.717
	3.59	J001957.99+591832.2	22.946	0.550	0.604
#10	1.09	J002011.91+591827.6	19.911	0.883	0.955
	2.51	J002011.55+591825.4	21.903	0.672	
	3.02	J002011.87+591829.7	22.798	0.438	
	3.74	J002011.76+591823.0	22.901	1.456	1.408
	3.95	J002011.59+591823.2	23.305	1.091	1.452
#11	3.78	J002012.61+591724.6	23.381	0.834	0.997
#15	0.97	J002022.52+591732.9	18.404	0.590	0.642
	1.81	J002022.17+591732.8	22.633	1.026	1.019
	2.46	J002022.33+591730.8	22.744	1.521	1.460
	3.52	J002021.99+591731.6	23.073	0.443	0.921
	3.60	J002022.40+591729.6	23.417	1.003	0.782
	3.82	J002022.20+591729.7	23.299	-0.084	
	#16	0.38	J002025.23+591807.3	20.857	1.409
0.46	J002025.14+591807.0	19.644	0.263	0.412	
1.29	J002025.36+591806.6	20.557	1.082	1.644	
1.40	J002025.05+591807.8	20.807	0.459	0.188	
1.64	J002025.41+591806.7	21.316	0.165		
1.92	J002025.24+591805.1	19.392	0.712	0.724	
1.97	J002025.33+591808.7	21.954	0.427		
2.04	J002024.95+591806.3	19.696	0.437	0.408	
3.14	J002025.60+591807.7	21.873	0.433	0.415	
3.39	J002025.45+591804.2	21.704	1.354	1.352	
3.43	J002025.04+591810.2	22.570	-0.150		
3.48	J002025.47+591804.2	21.753	1.400	1.355	

Notes. The LGGs ID in bold indicates the best match in terms of distance and infrared brightness.

LGGs stars fall within $4''$ of the silicate emission source coordinates, we selected the closest LGGs star. We list in Tables A.2 and A.1 the LGGs sources within $4''$ from each silicate emission candidate. We also list their optical colors. In all cases, the closest LGGs star is also the best match in terms of brightness and red color.